Macromolecular Chemistry and Physic
www.mcp-journal.d

Silk Fibroin-Based Films Enhance Rhodamine 6G Emission in the Solid State: A Chemical–Physical Analysis of their Interactions for the Design of Highly Emissive Biomaterials

Oktay K. Gasymov, Chiara Botta, Laura Ragona, Aytaj J. Guliyeva, and Henriette Molinari**

Described herein is the preparation of dye-doped films employing silk fibroin (SF) as a biomaterial, capable of preserving the optical properties of the monomeric dye in the solid state, a critical requisite for optical and biolaser applications. A comprehensive physical–chemical characterization is reported for SF films doped with Rhodamine 6G, an ideal candidate for photonics and optoelectronics. Fourier transform infrared spectroscopy (FTIR), circular dichroism (CD) and X-Ray diffraction (XRD) provide information on SF secondary conformation in the presence of rhodamine. UV–vis absorption spectra and exciton CD inform on the structure of encapsulated rhodamine, while changes in dye photophysical properties illuminate the molecular mechanism of the involved host–guest interactions. SF host environment inhibits rhodamine dimer formation, indicating that SF is an optimum matrix to keep rhodamine essentially monomeric at concentrations as high as 7 mM in the film. The relevant optical properties of these films and the easiness of their preparation, make these systems optimal candidates for innovative photonic technologies.

1. Introduction

Silk fibroin (SF), the predominant component of *Bombyx mori* silkworm cocoons, has become a popular biomaterial due to its excellent biocompatibility, exceptional mechanical properties, tunable degradation, ease of processing, and supply.[1,2] Silk fibroin is a structural protein consisting of heavy and light chains present in equimolar ratios with molecular masses of approx. 390 and approx. 25 kDa, respectively, bonded together by a single disulfide bond. The primary structure of SF consists of a predominance (approx. 90%) of the amino acids glycine, alanine, serine, valine, and tyrosine. Fibroins are composed of relatively large hydrophilic chain end blocks (N- and C-termini) and large internal hydrophobic regions including repetitive sequences of GAGAGS, GAGAGY, and GAGAGVGY, which are responsible for the formation of antiparallel β-sheets in the spun fibers.[3] The formation of β-sheets contributes to the stability and remarkable mechanical features of spun silk fibers. *B. mori* SF offers unlimited opportunities for functionalization, processing, and biological integration[4–8] thus representing a versatile tool for the preparation of biomaterials for regenerative medicine, tissue engineering, and a broad range of biomedical applications, as recently reviewed.[5] SF has also emerged as a suitable natural polymer for optics,[9–14] where new strategies are requested for the preparation of bioinspired host–guest complexes to be employed in technologically relevant applications, as sensors and optoelectronic devices.

Organic dyes, such as Rhodamine 6G (RHD), represent ideal candidates for photonic and optoelectronic applications, thanks to their excellent light-absorbing, fluorescence, and photosensitivity properties in the monomeric state. We have demonstrated that quenching effects, caused by the aggregation of pristine RHD in solution, can be efficiently reduced by encapsulating the monomeric RHD dye within a protein cavity, forming a water-soluble host–guest complex.[15] We have further shown that RHD, establishing specific interactions with SF in solution, is capable of inhibiting protein self-association, thus controlling β-conformational transition.[16] Now, the aim of the present paper is to investigate the physical–chemical properties of cast films, obtained by slow evaporation of SF solutions in the presence of different concentrations of RHD. Indeed SF films have been reported to display high transparency (approx. 95%) across the visible range, low surface roughness, biocompatibility, and tunable biodegradability.[10] These features could inspire the preparation of novel SF:RHD host–guest complexes, representing interesting nature-based materials for biophotonics.[17,18] Fourier transform infrared spectroscopy (FTIR), circular dichroism (CD) and X-Ray diffraction (XRD) have been here employed to provide information on the influence of RHD on SF structure, deconvolution of absorption spectra, together with exciton coupled CD spectroscopy, informed on the structure of encapsulated RHD in the different mixtures, providing evidence for a counterclockwise screw configuration of the interacting dimers. Changes in RHD photophysical properties (absorption and fluorescence (FL) spectroscopies)

Dr. O. K. Gasymov, A. J. Guliyeva
Institute of Biophysics of ANAS
117 Khalilov, AZ-1141 Baku, Azerbaijan
E-mail: ogassymo@ucla.edu
Dr. C. Botta, Dr. L. Ragona, Prof. H. Molinari
Istituto per lo Studio delle Macromolecole (ISMAC), CNR
via Corti 12, 20133 Milano, Italy
E-mail: henriette.molinari@ismac.cnr.it, henriettemolinari0@gmail.com
The ORCID identification number(s) for the author(s) of this article can be found under https://doi.org/10.1002/macp.201800460.

DOI: 10.1002/macp.201800460

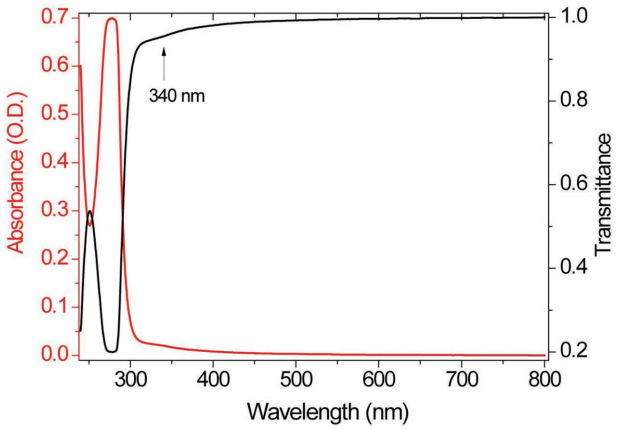

Figure 1. Absorption/transmission spectra of SF film with approx. 38 µm thickness. The maximum of the absorption was normalized to a value of 0.7 to evaluate transmittance values in the full spectral range. Film transparency was up to 95% in the visible region (390–700 nm).

afforded details of the involved host–guest interactions, whose knowledge is relevant for the fabrication of fluorescent based biodevices for optical and laser applications.

2. Results and Discussion

Transparent SF films were easily prepared by drop casting and slow drying methods, as reported in the literature.[19] The transmission spectrum obtained for the pristine SF film is reported in **Figure 1** while the images of films obtained at different SF:RHD ratios are reported in Figure S1, Supporting Information.

The physical–chemical properties of pristine SF and SF:RHD films, obtained at different protein:ligand ratios (see Experimental Section) have been thoroughly investigated, as described below.

2.1. SF Conformation in Films

FTIR is a useful tool to monitor SF conformational changes. Protein materials are characterized by the position and intensity of the amide I, amide II, and amide III bands occurring at 1630–1655, 1540–1520, and 1270–1235 cm^{-1}, respectively. FTIR spectra of silk fibroin films in the amide regions (1800–1200 cm^{-1}) are correlated with Silk I (1655, 1540, and 1235 cm^{-1}) and Silk II (1630, 1520, and 1270 cm^{-1}) content, an indicator of the conformational properties of the self-assembled proteins.[20–22] In addition to the commonly reported β-sheet and turn structures, it is also possible to identify a β-aggregated structure, which enhances the amide I band at 1615 cm^{-1}, due to the presence of intermolecularly hydrogen bonded β-sheets.[23] In order to investigate the effect of RHD on SF secondary structure, FTIR spectra were acquired for pristine SF and for films at SF:RHD molar ratios varying from 1:1.2 to 1:37 (**Figure 2**). FTIR spectra were also measured for an aqueous SF solution and for films obtained by water annealing and methanol (70%) treatment, two commonly used approaches to form β-sheet crystals[22] (Figure 2). Exposure to methanol favors the

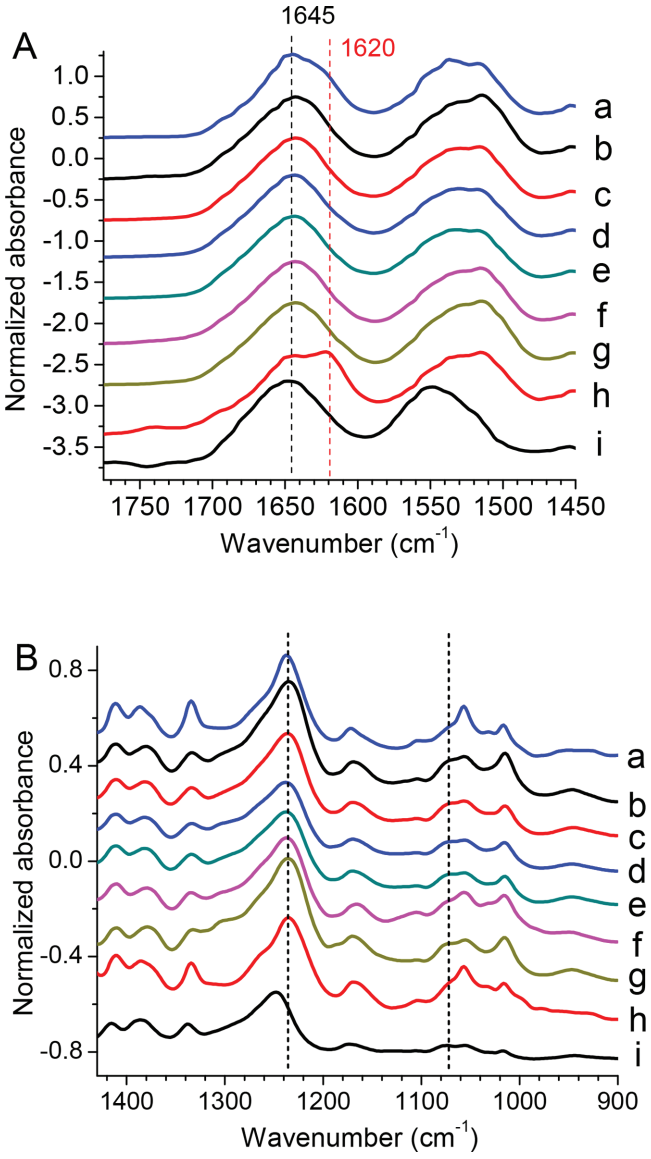

Figure 2. FTIR spectra, covering the spectral region of the A) amide I and II bands and B) amide III and side chain bands, obtained for SF films with different composition: a) SF film (from a 86 µM solution); b) SF film from a solution of SF:RHD 1:1.2; c) 1:2; d) 1:5; e) 1:9; f) 1:19; g) 1:37; h) SF film treated with 70% MetOH; i) SF solution (86 µM). Silk I and Silk II bands, occurring at 1645 and 1620 cm^{-1}, respectively, are indicated by black and red dashed lines in (A). In (B), the dashed line at 1240 cm^{-1} corresponds to amide III band while the dashed line at 1070 cm^{-1} does not correspond to any particular band and has been reported to highlight changes occurring upon increasing the RHD concentration. Formation of a new band at 1620 cm^{-1}, typical of β-sheet, is evident only in the presence of 70% MeOH.

conformational change from Silk I to Silk II,[22] with a threefold increase in β-sheet content when compared to water-annealed silk films.[12,24] FTIR spectra of SF and its different complexes with RHD do not show the appearance of new bands or an increase of some bands upon increasing RHD concentration from 100 to 3.2 mM, thus indicating that RHD itself does not contribute to FTIR spectra.

The fractional change of secondary structure as a function of added RHD can be assessed by deconvolution analysis, fitting the amide I curve, the most informative for the analysis of protein structures, to multiple Gaussian components.[23] It should be noted that fitting the amide I band to a varying number of components with diverse width sizes creates some uncertainties leading to subjectivity and errors in estimating the secondary structure content of proteins. Interestingly, a recently established method reported on a significant improvement in FTIR structural analysis,[23] showing that fixing the number of the peaks, their spectral positions and limiting the peak width range, significantly reduces the number of floating parameters and uncertainties. Deconvolution of the amide I bands of the films are reported in Figure S2, Supporting Information. Estimated contents of the secondary structure elements are shown in the **Table 1**. The total β-sheet content is higher in films (48.4%) with respect to solution (38.8%), while, as mentioned, 70% methanol treatment induces additional β-sheet formation (57.4%) (Table 1), in line with previously published data.[12] FTIR data indicate that the conformational properties of SF films display a dominance of Silk I (random coil and alpha-helices secondary structures) with respect to the Silk II conformation (β-sheet secondary structures), consistent with reported data,[21,23] while the addition of RHD (at all tested ratios) slightly decreases the total β-sheet structure in SF films. The component at 1615 cm^{-1} represents intermolecular β-sheet aggregate due to stacked β-sheets from different molecules, stabilized by side chain interactions, as observed in β-amyloids.[25,26] Amyloid size and rigidity determine the frequency of this band, with the largest and most rigid amyloids absorbing near 1620 cm^{-1} and the smaller, more disordered and less rigid amyloids absorbing at about 1635 cm^{-1}.[27] The β-sheet aggregate induced by alcohol in SF film can be considered as the largest and most rigid, making the film insoluble in aqueous solution. The existence of a component at 1693 cm^{-1} indicates that intermolecular β-sheet aggregates are composed of β-strands arranged antiparallel to each other.[27] FTIR spectral analysis indicates the presence of β-sheet aggregate (12.1%) that increased up to 22.9% by treatment with alcohol. SF films with various amount of RHD (from 1:1.2 to 1:37) contain 1.6–9.9% β-sheet aggregate. Water annealing or alcohol treatment of some SF:RHD films exhibited β-sheet aggregate in the range of 6.4–11%, always lower than the amount observed for SF films treated with alcohol. Interestingly, when SF:RHD films were subjected to repeated alcohol spray treatment for at least 2 h, an aggregated β-sheet structure was not observed, at variance with the behavior of pristine SF films. Altogether FTIR data clearly show that RHD inhibits the formation of intermolecular β-sheet aggregates, consistent with our previous findings on the role of RHD in preserving, in solution, non aggregated SF.[16]

The formation of intermolecular β-sheet aggregate in SF films upon alcohol treatment was also confirmed by CD spectroscopy (Figure S3, Supporting Information).

XRD data obtained for SF:RHD films provide further structural information, specific of the different silk conformation,[19,28,29] as they reveal spacing between atoms positioned in parallel planes provided as peak positions. Results obtained at different molar ratios are shown in **Figure 3** reporting, for comparison, the data for SF film treated with 70% methanol. Parameters obtained from deconvolution of XRD spectra are reported in **Table 2**. The spectra shown in Figure 3b–h are typical for semicrystalline polymers such as SF. The significant sharpening of peaks observed for SF film with 70% alcohol treatment indicates formation of a regular structure. However, in agreement with FTIR data, XRD confirms that there are minor differences in secondary structure of the films with and without RHD.

Methanol treatment leads to the formation of new maxima (4.5 Å spacing) with significant intensity specific of β-structure (Figure 3a). Deconvolution of XRD data for silk fibroin films treated with methanol also indicates formation of structures with spacing of 8.5 and 6.2 Å. In XRD diffraction pattern, d-spacing values of 9.8 and 4.3–4.5 Å (hydrogen-bonded interchain and intrahydrogen-bonded β-sheet spacing, respectively) indicates β-sheet formation.[19,30]

Table 1. Estimation of secondary structure elements for various SF films from deconvolution of amide I bands of FTIR spectra.

	1693 cm^{-1} intermolecular β-sheet (antiparallel)	1680 cm^{-1} β-turn	1656 cm^{-1} random coil	1644 cm^{-1} α-helix	1628 cm^{-1} intramolecular β-sheet	1615 cm^{-1} intermolecular β-sheet (aggregate)	1712 cm^{-1} side chain	Total β-structure
SF solution	0	18.2	35.4	25.9	17.3	3.3	0	38.8
SF film	0.4	15.2	31.4	20.1	20.7	12.1	0	48.4
SF film (70% alcohol)	1.7	13.5	27.9	14.8	19.3	22.9	0	57.4
SF: RHD (1: 1.2)	0.3	19.1	26.2	27.9	20.3	6.2	0	45.9
SF: RHD (1: 2)	0.2	19.0	26.3	29.1	23.8	1.6	0	44.6
SF: RHD (1: 5)	1.2	17.4	27.8	28.4	19.6	5.5	0	43.7
SF: RHD (1: 9)	0.8	18.7	28.7	28.3	20	3.5	0	43.0
SF: RHD (1: 19)	1.0	19.0	27.1	25.6	20.8	6.5	0	47.3
SF: RHD (1: 37)	0.4	18.3	26.5	25.4	19.4	9.9	0	48.0
SF: RHD (1: 9) (70% alcohol)	0.5	17.3	24.4	27.7	23.7	6.4	0	47.9
SF: RHD (1: 9) (water)	4.0	16.8	24.8	25.2	18.4	10.5	0.3	49.7
SF: RHD (1: 19) (70% alcohol)	1.6	19.5	27.8	24.1	15.8	11.0	0.1	48
SF: RHD (1: 19) (water)	0.8	20.8	23.9	24.3	18.4	11.0	0.9	50.9

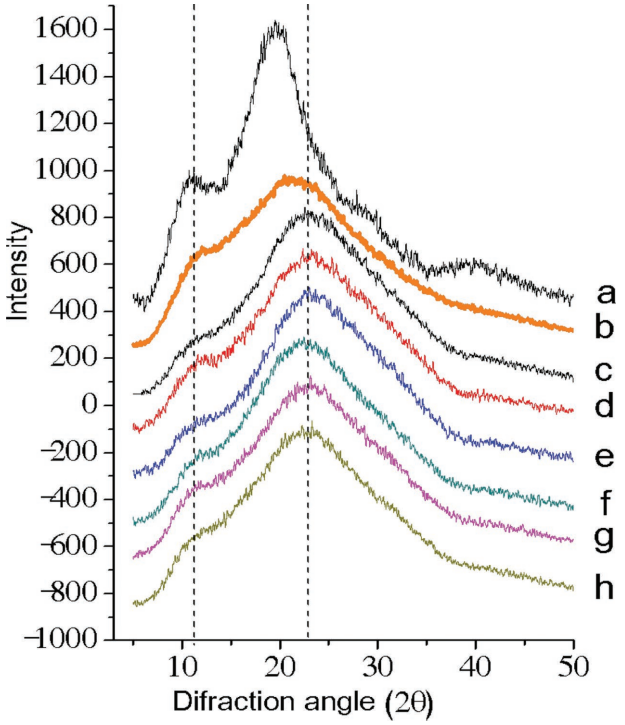

Figure 3. XRD data for various RHD:SF films (baseline corrected, area-normalized). a) SF film treated with 70% methanol; b) pristine SF film; c) SF:RHD 1:1.2; d) SF:RHD 1:2; e) SF:RHD 1:5; f) SF:RHD 1:9; g) SF:RHD 1:19; h) SF:RHD 1:37. XRD spectra are vertically shifted for better comparison.

2.2. RHD Aggregation State in SF Films

Absorption spectra of RHD:SF films can give useful information on the self-aggregation state of RHD dye in SF matrix. Data obtained at variable RHD:SF ratios are reported in **Figure 4**. The spectrum of a pristine SF film, collected in the 240–360 nm region (Figure S4, Supporting Information), shows a broad peak centered at 275 nm, corresponding to the predominant absorbance of tyrosine. Spectra recorded for SF:RHD ratios up to 1:5 exhibit two isosbestic points (at 518 and 556 nm), showing that the increased concentration of RHD is consistent with the presence of monomeric species (decrease of absorbance at around 538 nm) in equilibrium with H- and J-type dimeric species (increase of absorbance at around 508 nm). H- and J-dimers refer to different geometries, namely perfect sandwich or in-line head-to-tail dimers, respectively.[31,32] Formation of high-order aggregates at these ratios is not probable, in analogy with data reported for RHD incorporated in solid thin films of laponite clay, where the formation of high-order aggregates, upon increasing the concentration of RHD, leads to the disruption of both isosbestic points.[31]

In SF films at SF:RHD 1:9 and higher ratios, the isosbestic point at 518 nm is smeared, possibly due to the formation of a component with a broad spectrum contributing to the spectral region at lower wavelengths. Higher order nonresolved components of RHD may be responsible for this broad spectrum. At variance, the isosbestic point at 556 nm is maintained, indicating the formation of a J-type dimer. The absorption band of J-type dimer occurs at about 546 nm (in our case 565 nm). Appearance of spectral components with maximum absorption at 565 nm leads to an isosbestic point at 556 nm, consistent with the transition of monomer to J-dimer.

Interestingly, in solution, RHD shows two isosbestic points, one at 508 nm, which is not disrupted up to an RHD concentration of 128 μM and one at 552 nm, which remains up to RHD concentration of 4.1 mM. This suggests that monomer to high energy H-dimer (isosbestic point of 508 nm) and to low energy J-dimer (isosbestic point of 552 nm) transformations remain equivalent up to 128 μM and 4.1 mM concentration of RHD, respectively. Disruption of isosbestic point at 508 nm at concentration higher than 128 μM indicates formation of higher oligomers.[33] Indeed it is expected that specific RHD-silk fibroin interactions may modify the dimer formation of RHD incorporated into silk fibroin.

The contribution of RHD monomeric species in the films can be estimated from the deconvolution of absorption spectra. Up to SF:RHD equimolar ratio the amount of monomeric species can be considered as 100%. The contributions of monomeric RHD for films obtained at SF: RHD 1:2, 1:5, 1:9, and

Table 2. Parameters obtained from the deconvolution of XRD spectra of the various films to Gaussian components. Peaks and the corresponding area values were determined from Gaussian (four peaks) peak fitting of corrected XRD data (baseline correction and area-normalized).

Film	Pick1 [Å]	Area 1	Pick 2 [Å]	Area 2	Pick 3 [Å]	Area 3	Pick 4 [Å]	Area 4
SF film	7.8	1247	4.2	10 839	2.8	747	2.3	2065
SF:RHD (1:1.2)	7.8	1190	3.9	10 100	2.8	1988	2.2	1131
SF:RHD (1:2)	7.8	1095	3.9	10 800	2.8	1423	2.2	1350
SF:RHD (1:5)	7.6	1134	3.9	9657	2.8	2004	2.2	1861
SF:RHD (1:9)	7.9	932	4	10 916	2.8	1276	2.2	2006
SF:RHD (1: 19)	7.8	1144	3.9	11 119	2.8	844	2.3	1911
SF:RHD (1:37)	7.9	1081	4	11 564	2.8	864	2.3	1862
Average of above films	7.8 ± 0.1	1118 ± 99	4.0 ± 0.1	10 714 ± 638	2.8 ± 0	1307 ± 530	2.2 ± 0.1	1741 ± 355
SF film (MetOH)[a)]	8.5 6.2	1554 2391	4.5 3.6	6983 385	3.2	3649	2.3	1873

[a)]Six Gaussian components were necessary for the satisfactory fitting of XRD data of SF film treated with MetOH.

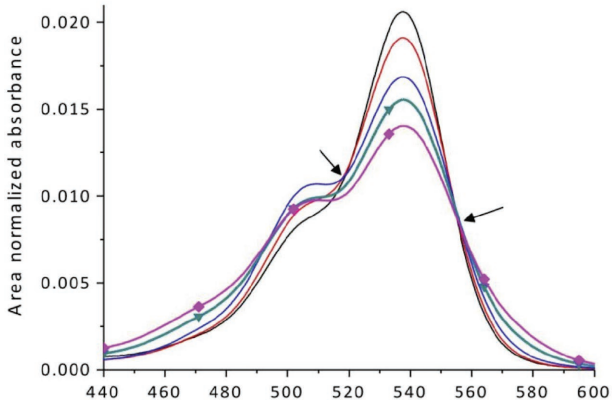

Figure 4. Area-normalized absorption spectra of SF:RHD films obtained at SF:RHD variable ratios 1:1.2 (black), 1:2 (brown), 1:5 (blue), 1:9 (green), 1:19 (pink). The two isosbestic points occurring at 508 and 556 nm are indicated with arrows.

1:19 ratios are 90.5%, 72.8%, 58%, and 43.9%, respectively. These data clearly show that SF is an optimum matrix to keep RHD monomeric at high concentrations. As an example, for the preparation of films at SF:RHD 1:5, a 400 μM RHD solution has been employed. During SF solution-to-film formation, the SF volume decreased 40 times, with RHD concentration expected to increase accordingly, reaching a concentration close to 16 mM. Thus, it can be concluded that binding of RHD to SF, at SF:RHD lower than 1:9, strongly inhibits the formation of RHD dimers and higher oligomers, leading to higher fluorescence yields (see later), an important requirement for the preparation of good laser material.

Application of exciton theory provides the geometry of RHD J-dimers in silk fibroin films.[31] Thus, calculations performed for the film at SF:RHD ratio of 1:9, where J-dimers are clearly identified, (**Figure 5** and **Table 3**) indicates the presence of an oblique head-to-tail dimer with a intermolecular distance of 8.6 Å and a torsional angle (**Scheme 1**) of 109.4°. Table 3 reports the deconvolution of the absorption spectrum at SF:RHD ratio of 1:9, indicating the relative content of the components. Surprisingly, water and alcohol annealing of the film resulted in loss of J-type dimers and increase of H-type dimers.

The interaction energy between monomeric units in the dimer has been estimated to be about 1071 cm^{-1}. These figures are consistent with those obtained for RHD dimers in solid thin films of laponite clay ($U = 785$ cm^{-1}, $R = 9.5$ Å, $a = 109°$).[31] The limitation of interlayer distance in solid films is expected to prevent the piling-up of parallel RHD planes, as suggested for clay laponite.

It was previously shown that H-dimers are not fluorescent, but are good fluorescence quencher of monomeric species via

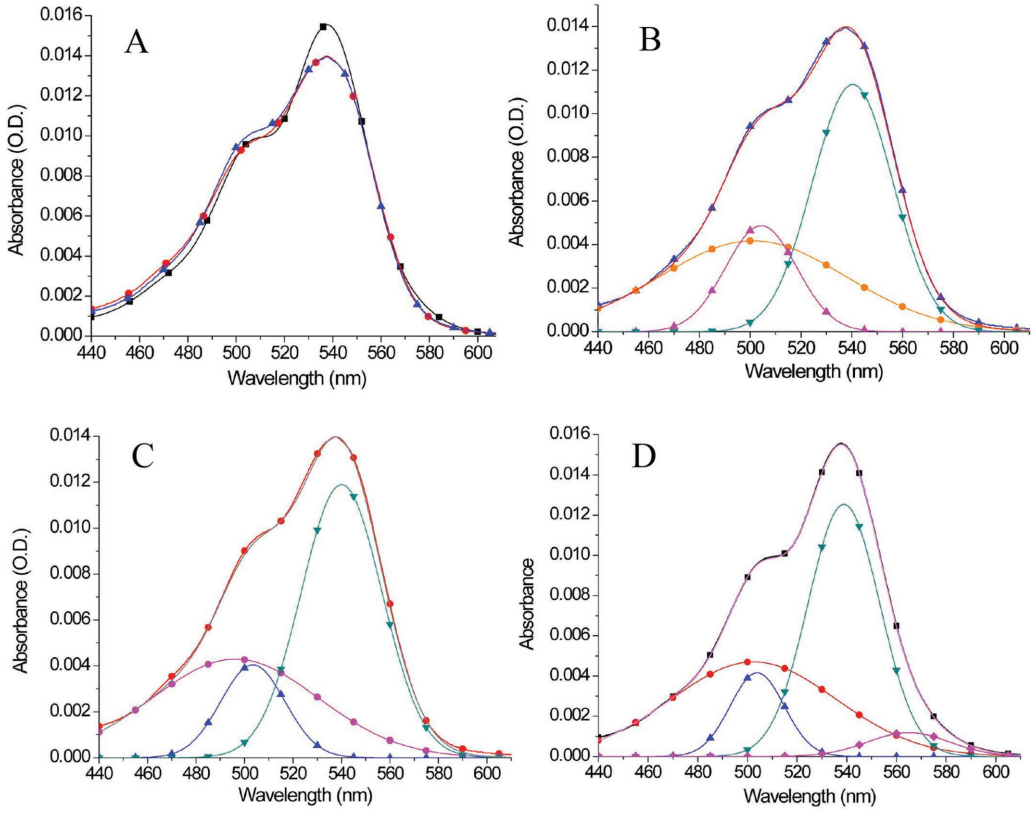

Figure 5. Area-normalized absorption spectra of SF:RHD at 1:9 ratio and their Gaussian components in various conditions. A) SF:RHD film (black square); SFD:RHD film treated with 70% alcohol (red circle); SF:RHD film after water annealing (blue triangle); B) fitting of the absorption spectrum of SF:RHD film annealed with water to Gaussian components. C) Fitting of the absorption spectrum of SF:RHD film treated with 70% alcohol to Gaussian components. D) Fitting of the absorption spectrum of SF:RHD film to Gaussian components.

Table 3. Results of the deconvolution of UV absorption spectrum at SF:RHD ratio of 1:9, indicating the relative contents of the different components.

	≈539 nm monomer	≈504 nm H-dimer	≈565 nm J-dimer	496–502 nm higher aggregates
SF: RHD 1:9	0.454	0.113	0.049	0.380
SF: RHD 1:9, 70% EtOH	0.497	0.134 (+18.8%)		0.350
SF:RHD 1:9 water	0.450	0.171 (+ 51.3%)		0.360

electron transfer mechanism. This is an important issue to be taken in consideration when analyzing fluorescence data (see later).

Exciton coupled CD spectroscopy can provide further information on the structure of encapsulated RHD. In chiral substances, through-space coupling of two or more identical chromophores, which are in close proximity and favorable orientation, gives rise to exciton-coupled circular dichroism, that is, exciton CD. Exciton CD spectra have characteristic bisignate curves (couplet), the sign of which reflects the chirality between the electric transition moments of interacting chromophores.[34–37] The sign of the long wavelength band of exciton CD determines the sign of the couplet. The electronic CD exciton chirality method defines that negative exciton CD comes from the situation where the long axes of two chromophores constitute a counterclockwise screw. The opposite is true for the positive exciton CD. Far-ultraviolet (UV) CD spectra of proteins are mostly consequence of exciton interactions of the amide groups of the polypeptide backbone of proteins[38] but exciton CD spectra are also observed for proximate Trp/Tyr residues.[35,39–41] The strength of exciton CD depends on the square of the oscillator strength, related to the molar extinction coefficient of the interacting chromophores. Thus the exciton CD for Trp/Tyr couples is not observed for L_a or L_b band (ε_{max} is about 4500 M^{-1} cm^{-1}), but for B_b band (ε_{max} is about 35 000 M^{-1} cm^{-1}). RHD with a molar extinction coefficient above 100 000 M^{-1} c^{-1} is thus well situated to observe exciton coupling. CD spectra of SF:RHD films with 1:2 and 1:5 ratios and their absorption spectra are shown in the **Figure 6**. The negative exciton CD couplet centered at 546.0 nm is evident for the SF:RHD (1:5) film. The couplet could unambiguously fit to almost perfectly symmetric two Gaussian peaks with opposite signs with maximum at 537.0 nm and minimum at 554.1 nm (dotted lines). The couplet center (546.0 nm, Figure 6A) is significantly shifted from the nearest maximum of absorption band (536.5 nm, Figure 6B), which belongs to monomeric RHD. Thus, bisignate couplet originates from J-type dimer (positioned at longer wavelength from maxima of monomeric RHD). The additional CD band with apparent maximum at 498.4 nm could be fit both to one Gaussian peak and two Gaussian peaks with opposite signs. Therefore, this band could not be unambiguously assigned to bisignate exciton CD. However, there are additional features that may help the interpretation of this band. First of all, the maximum at 498.4 nm does not match with the maximum of any band in the respective absorption spectra. The nearest band in absorption spectra occurs at about 503 nm. Second, the CD spectrum of SF:RHD (1:2) film shows only one negative band with very weak intensity, despite that the absorption values for

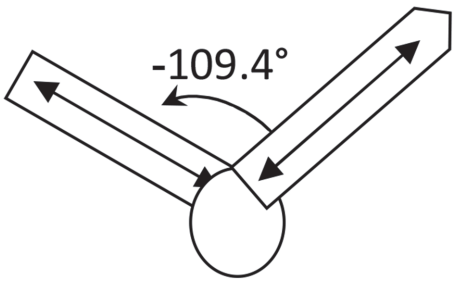

Scheme 1. Drawing of the oblique head-to-tail J-dimer. The torsional angle between the transition moments of the monomers in the dimer is indicated. Evidence for counterclockwise screw configuration is provided by CD results (see further).

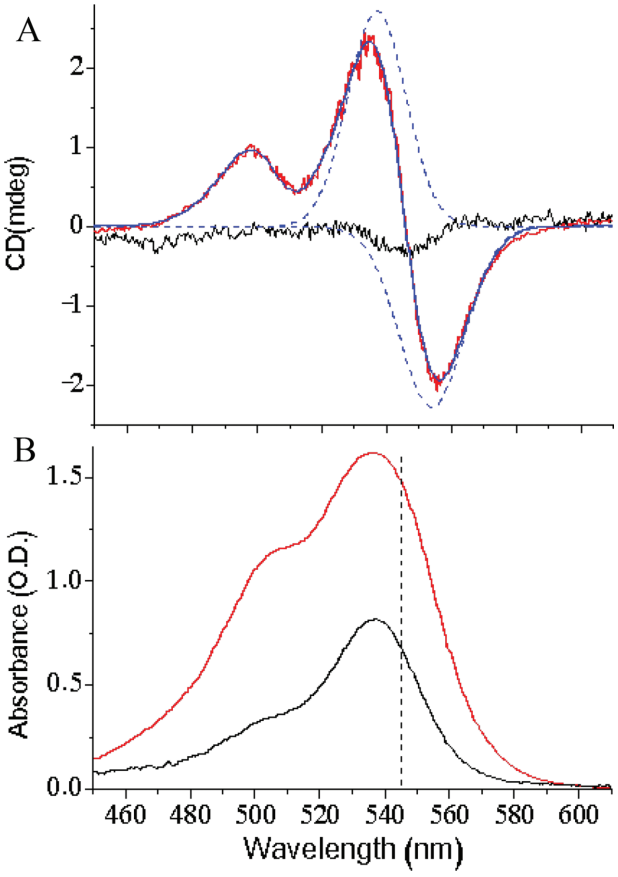

Figure 6. Exciton coupled CD of RHD dimers incorporated in SF films. A) CD spectra of SF:RHD 1:2 (black line) and 1:5 films (red line). Fit to Gaussian peaks (solid blue line), Gaussian components of negative coupled band (dotted blue lines). B) Absorption spectra of the above-mentioned films simultaneously measured with CD [color codes are the same as in (A)]. The vertical dashed line shows the position of the exciton CD couplet center.

the SF:RHD film at 1:5 molar ratio (at 537 and 508 nm) are two and three times higher, respectively, compared to those for the SF:RHD film at 1:2 molar ratio. Thus CD spectra intensities are not related to the corresponding absorbance values. Both bands of the CD spectrum of SF:RHD 1:5 film refer to the interacting RHD dimers. Based on all these considerations, the apparent maximum at 498.4 nm can be assigned to RHD H-dimer, indicating that the exciton coupled CD spectrum of SF:RHD (1:5) film can provide evidence of interacting RHD dimers. In addition, the negative sign of the exciton coupled CD indicates that the long axes of two interacting RHD molecules in the dimer constitute a counterclockwise screw (Scheme 1).

2.3. Investigation on Host–Guest Interactions

Fluorescence emission spectra of SF:RHD films with different relative molar ratios varying from 1:0.5 to 1:19 (**Figure 7**) were obtained upon excitation of tyrosine (275 nm) and tryptophan (300 nm), while the main fluorescence properties are summarized in **Table 4**. Tyr emission is observed at 302 nm for all the films while the RHD emission maxima shift from 558 to 594 nm upon increasing the RHD content. An additional blue fluorescence at 420–450 nm, already reported in the literature,[42] and more evident by exciting at 300 or 407 nm (Figure 7b and Figure S5, Supporting Information), is observed in all the films. It has been shown that crosslink formation in SF solutions induces a broad emission in the 390–407 nm region, that is significantly enhanced and red-shifted in the blue region in gels.[43] The origin of this blue fluorescence is not clear, as there may be more than one type of crosslink involved when the β-sheets acquire a stacked conformation. Oxidized tryptophan is one possible contributor but fluorescence in the same spectral region can be originating from dityrosine crosslinks.[44] Thus it was assumed that noncovalent and stacking interactions between tyrosine, tryptophan, and potentially other protein components, enhanced during β-sheet formation, contribute to the blue fluorescence emission. Figure 7 reports the emissive properties of a cast film of the pure dye (SF:RHD 0:1), deposited in the same way as the other films. This film displays a broad and very weak emission with QY below the instrument sensitivity (see Table 4). These features are related to the large inhomogeneity of the dye aggregation states that gives emissions in different spectral regions, combined with the quenching due to energy transfer to lower energy nonemissive H-aggregates. At variance, SF:RHD films with molar ratios up to 1:10 show much narrower RHD emission spectra, representative of the SF ability to reduce RHD aggregation, as discussed later.

In order to study the fluorescence properties of the films we have measured the decay times of both the RHD fluorescence (560 nm) and the blue SF fluorescence (450 nm) by exciting at 407 nm films containing different SF:RHD ratios (**Figure 8**). The decay of the RHD emission displays a quasi-monoexponential behavior for low RHD concentrations (SF:RHD 1:0.5 and 1:1.2 ratios; see later for the detailed analysis of lower concentrations), while at higher RHD concentrations the decays become nonexponential with a reduction of the average RHD lifetimes (Table 4 and Figure 8). The strongly nonexponential decay observed for the pure dye (SF:RHD 0:1) and the long-lived tail in its decay profile (see Figure 8B) is typical of weakly emissive Rhodamine 6G aggregated states.[45] This result confirms our hypothesis that at low RHD content (SF:RHD up to 1:1.2) the formation of RHD dimers and higher oligomers is suppressed while at high RHD concentrations (SF:RHD 1:5 or higher) the formation of RHD H-aggregates are responsible for the reduction of both lifetimes and quantum yields (QYs) of the dye.[46] It is worth noting that the quantum yields of SF:RHD 1:1.2 and 1:5 samples varies substantially (see Table 4), even if their crystallization level (indicated by β-sheet content) is similar (see Table 1 and Table 2), clearly indicating that optical and fluorescence properties of these films depends on the presence of dimers and higher order aggregates.

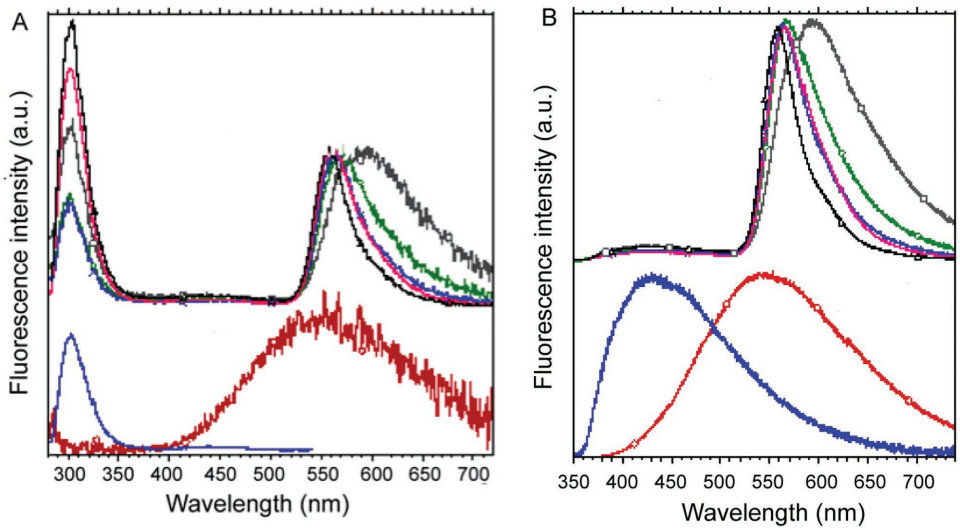

Figure 7. Normalized fluorescence spectra of the films excited at A) 275 nm and B) 300 nm. In both panels, different SF:RHD ratios are represented by colored lines: SF:RHD 1:0.5 black, SF:RHD 1:1.2 fuchsia, SF:RHD 1:5 blue, SF:RHD 1:10 green, SF:RHD 1:20 gray (upper part of the panels); SF:RHD 0:1 red, SF:RHD 1:0 blue (lower part of the panels).

Table 4. Fluorescence emission maxima and average lifetimes of the films.

SF:RHD	λ_{em} [a)] [nm]	λ_{em} [b)] [nm]	λ_{em} [c)] [nm]	QY[d)]	τ_{av} [ns][e,f)]
1:0	302	430			8.95[b)]
1:0.5	302	425	558	0.41	2.80[e)]
1:1.2	302	425	565	0.47	2.70[e)]
1:5	302	425	564	0.10	1.23[e)]
1:9	302	425	567	0.05	0.82[e)]
1:19	302	425	594	0.02	1.07[e)]
0:1			546	<0.01	<0.2[e)]

[a)]SF emission, λ_{exc} = 275 nm; [b)]SF emission, λ_{exc} = 300 nm; [c)]λ_{exc} = 300 nm; [d)]λ_{exc} = 488 nm; [e)]λ_{exc} = 407 nm; [f)]λ_{em} = emission maxima.

It should be noted that, even when embedded RHD is aggregating (SF:RHD 1:5), an increase of one order of magnitude in quantum yields is observed with respect to pristine RHD film (Table 4), thus showing SF capability to interfere with RHD aggregation.

The analysis of the decays of the SF blue emission indicated that no sensitive variations are observed at SF:RHD ratios of 1:0.5 and 1:1.2 with respect to the pure SF film, while at SF:RHD ratios equal or higher than 1:5 (when H-aggregates are formed) the SF blue emission undergoes a strong quenching. The fluorescence excitation profiles of the RHD emission display, for all the films (Figure S6, Supporting Information), a peak at 276 nm associated to Tyr, indicating that energy transfer from SF to RHD occurs at all the concentrations. The variations observed in the profiles for high RHD concentrations are consistent with the appearance, in excitation spectra (increase of the 505 nm shoulder), of nonfluorescent H-aggregates that transfer their energy to the low energy J-dimers.[46] The strong reduction in the average lifetimes of the SF blue emission observed at 1:5 or higher RHD ratios can be explained by energy transfer to nonemissive RHD H-aggregates, whose absorption overlaps with the blue SF emission, satisfying the condition for Forster resonance energy transfer[47] (Figures S5 and S6, Supporting Information).

Significant deviation of RHD concentration dependent quenching data for quantum yield and lifetime values indicates substantial formation of RHD aggregates. Quenching of quantum yield data (Equation (1)) influenced both dynamics (quenching during the lifetime) and static quenching (complex of molecules where quenching occurs before the fluorescence event). However, relative decrease in the lifetimes (Equation (2)) depends only on dynamic quenching. Obviously, nonfluorescent aggregates of RHD do not contribute to fluorescence intensity decay.

$$F_0/F = \left(1 + K_D[Q]\right)\left(1 + K_S[Q]\right) \quad (1)$$

$$\tau_0/\tau = \left(1 + K_D[Q]\right) \quad (2)$$

where F is the fluorescence intensity or quantum yield, K_D is the dynamic quenching constant, K_S is the static quenching constant, Q is the concentration of the quencher (dimer or higher aggregates of RHD in our case). Index 0 in F_0 and τ_0 indicates the situation without quencher.

Thus, in agreement with the results described above, data of Table 4 and Figure S7, Supporting Information (reporting the concentration dependence of RHD fluorescence quantum yield and lifetime in the analyzed films) indicate that RHD aggregate formation is the major mechanism of the quenching events in films containing high dye concentration (SF:RHD 1:5 or higher). However, other quenching mechanisms at work at low RHD concentration (where the dye is monomeric) cannot be ruled out and will be analyzed in the following.

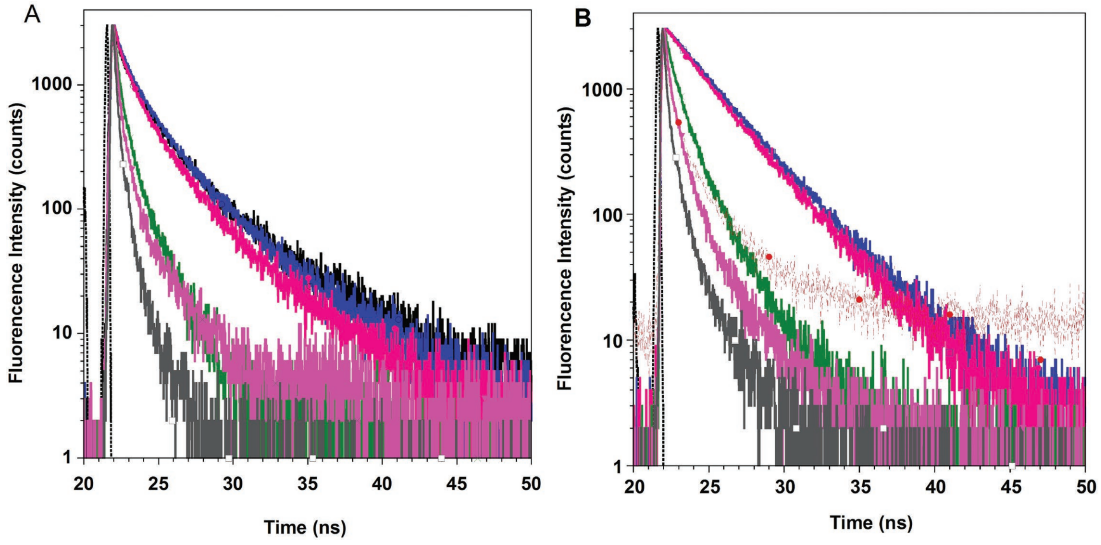

Figure 8. Fluorescence decays of RHD:SF films for emissions at A) 450 nm and B) 560 nm, excited at 407 nm. In both panels, different SF:RHD ratios are represented by colored lines: SF:RHD 1:0 black, SF:RHD 1:0.5 blue, SF:RHD 1:1.2 fucsia, SF:RHD 1:5 green, SF:RHD 1:9 pink, SF:RHD 1:19 gray, SF:RHD 0:1 red.

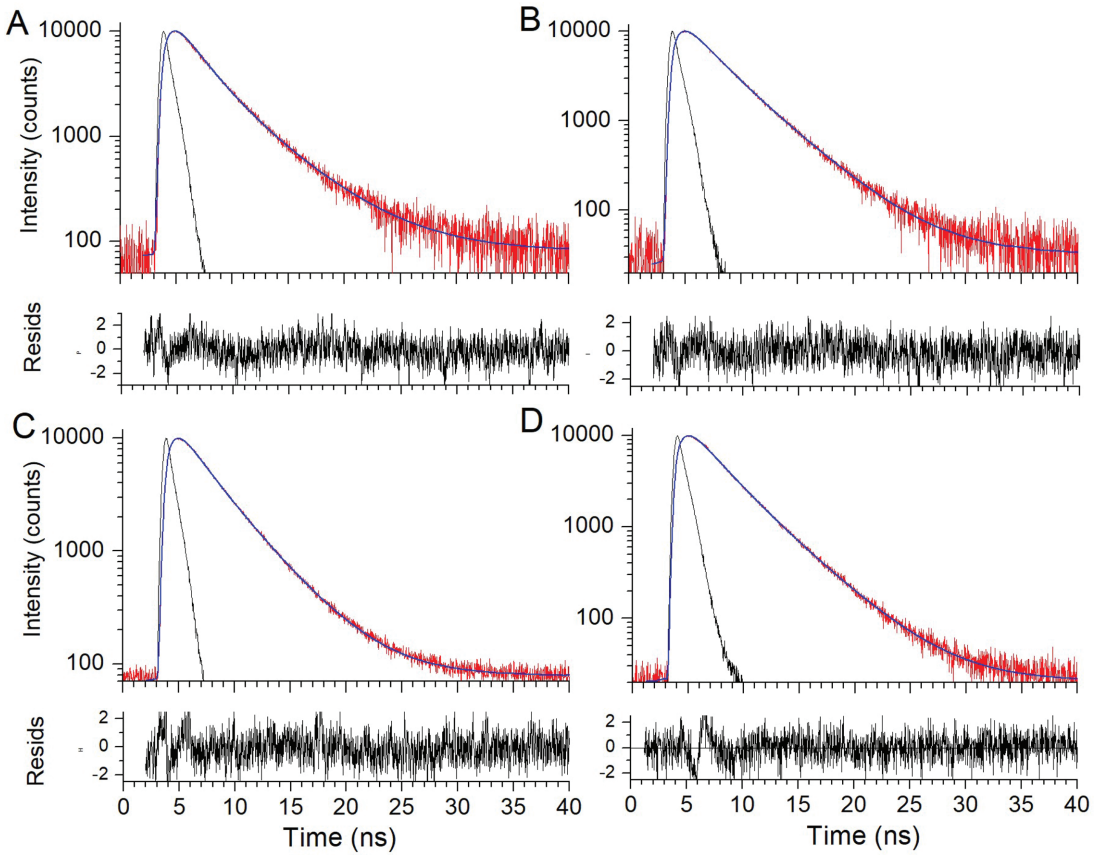

Figure 9. Fluorescence decay curves (red lines) for the films with low RHD concentrations. A) SF:RHD (1:0.005); B) SF:RHD (1:0.02); C) SF:RHD (1:0.2); D) SF:RHD 1:0.2 hydrated sample. Solid black lines represent instrument response function (IRF). Solid blue lines indicate the best fit for the double exponential decay model.

Fluorescence intensity decay measurements of SF films containing relatively low concentration of RHD (SF:RHD films at 1:0.005, 1:0.02, and 1:0.2 ratios) were also performed in order to verify the presence of short lifetime components of RHD fluorescence, which would clarify the origin of the observed quenching (**Figure 9** and **Table 5**). In all three samples (devoid of RHD dimers) along with lifetime components of 4.91–3.75 ns, relatively low (quenched) lifetime components (1.71–2.13 ns) are observed. Tryptophan and tyrosine residues are known to quench organic dyes, including RHD, via photoinduced electron transfer.[48] Thus the population of RHD with low lifetimes likely originates from fluorescence quenching by these aromatic side chains, as the H-dimers (fluorescence quenchers) are not formed at this low RHD concentration. Energy transfer from tyrosine to RHD, identified from excitation spectra of SF:RHD film (Figure S6, Supporting Information), indicates close proximity of these groups. In addition, the relative population of the low lifetime components (pre-exponential values) is decreased at higher RHD concentrations (up to 1:0.2), in agreement with the presence of specific binding.

RHD amplitude-averaged lifetimes, which are proportional to the quantum yield, are almost identical (Table 5), indicating that the relative population shift, upon increasing RHD concentration, preserves the quantum yield, which bears relevance for laser application.

Time-resolved measurements, repeated for an hydrated SF:RHD 1:0.2 sample (Table 5) showed that τ_1 and τ_2 lifetimes are increased (about 33% and 7% for short and long lifetimes, respectively) with a concomitant rearrangement in the populations of RHD molecules having short and long lifetimes. Interestingly, the most important outcome of the time-resolved measurement on the hydrated sample is that amplitude-averaged lifetime, which reflects steady-state intensity and therefore quantum yield, does not decrease. This result clearly shows that SF:RHD films are good laser material even in hydrated forms.

It should be further mentioned that high quantum yield value of a dye, regardless in solution or solid state, is the most important property for laser application. Up to 40-fold increase in RHD concentration, a decreased population of the relatively short lifetime component (from 0.64 to 0.32) and the concomitant increase of the relatively long lifetime component (from 0.36 to 0.68) maintain fluorescence quantum yield value. Thus, SF:RHD system is good for laser application over a wide range of the dye concentrations. RHD exciton CD indicates that at SF:RHD 1:5 or higher, where quantum yield values are substantially decreased, the formation of RHD dimers takes place with fluorescence intensity quenching of the monomeric RHD.

In order to assess the potentiality of SF:RHD films in the field of optoelectronics, our attention has been further focused on the properties of the RHD emission (fluorescence

Table 5. Fluorescence decay parameters for the SF:RHD films with low concentration of RHD.

SF:RHD	α_1[a)]	τ_1[a)]	α_2[a)]	τ_2[a)]	τ_{aver}[b)]	$<\tau>$[b)]	χ^2
1:0.005	0.64 ± 0.01	2.13 ± 0.04	0.36 ± 0.01	4.91 ± 0.07	3.69	3.13	1.21
1:0.02	0.39 ± 0.01	2.13 ± 0.06	0.61 ± 0.01	4.06 ± 0.04	3.57	3.30	1.07
1:0.2	0.32 ± 0.01	1.71 ± 0.04	0.68 ± 0.01	3.75 ± 0.01	3.39	3.10	1.15
1:0.2[c)]	0.49 ± 0.01	2.27 ± 0.03	0.51 ± 0.01	4.02 ± 0.02	3.44	3.19	1.08

[a)] α_i and τ_i are the normalized preexponential factor and decay time, respectively; [b)] τ_{aver} and $<\tau>$ are mean- (intensity-averaged) and amplitude-averaged lifetimes, respectively; [c)] Hydrated sample as described in the Experimental Section. Water content was determined to be 11%, in agreement with literature data.[58]

bandwidth, fluorescence quantum yields and lifetimes) in the films. The data reported in Table 4 show, for films obtained at SF:RHD 1:0.5 and 1:1.2, emission properties close to those of molecularly dispersed RHD, demonstrating that the amount of RHD aggregates in these films is lower with respect to similar films in standard matrices.[49] Indeed the results are comparable with those obtained by embedding RHD in solid state matrices, which require more complex preparation methods, as is the case for RHD in cellulose microparticles[50] or RHD encapsulated in Bile acid Binding Protein.[15]

3. Conclusion

The extensive physical–chemical characterization of SF films in the presence of different amounts of RHD allowed deriving some key features of the host–guest relationship, relevant for the application in the field of bio-optical devices. The films obtained with different SF:RHD ratios, as is the case for pristine SF films, are homogeneous and do not show any abrupt change in refraction indexes, which is reflected in the transparency of the films. Rhodamine 6G, acting as a guest, binds to its SF host preventing intermolecular β-aggregate arrangement of fibroin, even in the presence of methanol treatments. SF establishes specific host–guest interactions with RHD, through tyrosine and tryptophan side chains, inhibiting RHD dimer formation at SF:RHD concentration below or equal to 1:1.2. The contributions of monomeric RHD are still higher than 90% in films at SF:RHD 1:2 ratio, confirming that SF is an optimum matrix to keep RHD monomeric at high concentrations, a requisite for most optical and biolaser applications. At SF:RHD 1:5 (or higher) molar ratios the formation of RHD dimers is the major quenching mechanism of monomeric RHD fluorescence, substantially decreasing the film emission quantum yields. Thus it can be concluded, from the comparison of the properties of all the samples evaluated, that the optimal balance between photoluminescence intensity and film concentration for optical applications is at SF:RHD ratio between 1:1.2 and 1:2. Specifically at SF:RHD higher than 1:5 exciton coupled CD spectra provide direct evidence for the formation of interacting dimers with a counterclockwise screw configuration. It is worth noting that the observed concentration dependent fluorescence spectral shifts makes SF:RHD films appropriate for tunable solid state laser development.

Other SF:Rhodamine films have been previously reported in the literature[18,51–53] for the development of optical devices. However, most of them were prepared specifically for laser applications on structured substrates or contained other additives, thus preventing a direct comparison with our films. It is important to stress here that the properties that make silk interesting as a host for fluorescent dyes are mainly related to its biocompatibility, transparency, flexibility, and easiness of fabrication in any type of shape and dimension.

In addition other host materials have been successfully employed for embedment and control of intermolecular interactions.[54,55] Particularly relevant are those hosts able to impose specific spatial and geometrical organizations to the guests, such as organic and inorganic nanochannel forming systems,[55–57] since efficient funneling of the excitation toward a desired site (i.e., J-aggregates) can be easily realized.

Considering all the relevant SF:RHD film properties, here outlined, combined with their easiness of preparation, as compared to other bio host–guest systems, it can be concluded that the use of silk to bridge the worlds of optics and biology opens opportunities for a new and wide class of innovative bioinspired optical and photonic technologies, such as sustainable fluorescence-based lab-on-a-chip devices comprising fluorescence sensing platforms, and laser devices.

4. Experimental Section

Preparation of Silk Fibroin Films: *B. mori* silk cocoons were cut into fourths and boiled for 45 min in 0.02 M Na_2CO_3 (Sigma-Aldrich) to extract the glue-like sericin proteins from silk fibroin, as previously described.[5,16] The fibroin extract was then rinsed three times in Milli-Q water, dissolved in 9.3 M LiBr solution at room temperature, and set covered within a 60 °C oven for 4 h. The solution was then dialyzed in phosphate buffer 30 mM, pH 7.5 for 24 h. The dialyzed silk solution was then centrifuged for 10 min at 9000 rpm, and the supernatant was collected and stored at 4 °C. The final concentration of aqueous silk solution was 86 µM, as determined by UV absorption using extinction coefficient ε_{275nm} = 1.064 cm^{-1} mg^{-1} mL.[16] The films were obtained by slow evaporation of 400 µL SF solutions, deposited on polystyrene substrates, without and with different amounts of RHD 6G (Sigma-Aldrich N°252433). SF:RHD films at 1:0.005, 1:0.02, 1:0.2, 1:0.5, 1:1.2, 1:2, 1:5, 1:9, 1:19, 1:37 molar ratios were obtained employing RHD concentrations calculated with respect to a 86 µM SF solution. (In Figures 2, 3 and Tables 1, 2 the 1:37.2 molar ratio was summarized as 1:37). Each biophysical measurement was obtained with the selected SF:RHD molar ratios, as reported in the text. Specifically, SF:RHD samples at low molar ratios (1:0.005,1:0.02, and 1:0.2) were prepared and employed only to verify the presence of short lifetime components of RHD fluorescence, in order to clarify the origin of the observed quenching.

Pristine aqueous 400 µM RHD, corresponding to the RHD concentration in the SF:RHD 1:5 sample, was employed based on previous results,[16] showing that a stoichiometry of five was observed in solution for RHD binding to SF.

The dye concentration in dried films can be derived by considering the observed 40-fold volume reduction upon film formation (see text).

Alcohol Treatment of SF Films: For pristine film, the fibroin film was submersed in 70% MeOH solution for 1 h. The SF:RHD films were treated with 70% MeOH spray, to prevent removal of RHD from the films. After drying of the thin alcohol layer in air, films were repeatedly treated with alcohol sprays for 2 h. Both sides of the films were subjected to the alcohol spray.

Preparation of the Hydrated Samples: Samples have been treated by water spraying, in order to increase the water content of the films. Spray was continued until films were very flexible. Samples have been positioned between two quartz plates, with a teflon spacer of 0.3 mm and it was ensured that the sample did not dry during the measurements by sealing it, as shown in Figure S8, Supporting Information. The water content was measured by weighting the sample, in order to obtain data for dry and fully hydrated samples. The 11% water content measured for the sample, well corresponds to a fully hydrated sample, on the basis of literarture data[58] showing that the highest water content (12.6 ± 1.6 wt%) of the SF film occurred when the film was incubated at 25 °C for 48 h under a relative humidity of 84%. Both steady-state and time-resolved measurements were performed on the hydrated samples. In the steady-state measurements, the sample was equilibrated for 1 h before measurement to ensure that there were no intensity and fluorescence maxima changes. Fluorescence wavelength maximum was around 556.7 nm.

Measurement of Silk Fibroin Film Thickness: Silk fibroin film thickness data were obtained using vertical-type optical meter (IZV-2N710133, Russia).

FTIR Spectroscopy: Silk film secondary structural analysis was measured using a BioATR cell of the FTIR spectrometer (VERTEX 70v with CONFOCHECK system, Bruker, Inc., Germany). For each sample 256 scans were collected at a resolution of 2 cm^{-1} and acquired over a wavenumber range of 400–4000 cm^{-1}. Spectral manipulations were performed with OriginLab software (OriginLab Corp., Northampton, MA). Quantification of the SF secondary structure was based on the analysis of the amide I region (1600–1700 cm^{-1}). In the case of fibroin solution, background absorption due to water was subtracted from the sample spectra to obtain a flat recording in the range of 1750–2000 cm^{-1}. The amide I region (1580–1710 cm^{-1}) was selected from the entire spectrum, and a linear baseline was applied to the spectrum.

CD Spectroscopy: Spectra were recorded using a Chirascan V100 (Applied Photophysics, UK) circular dichroism spectrometer. Far-UV CD measurements were recorded from 260 to 190 nm with step size of 0.5 nm and bandwidth of 1 nm. SF films were prepared from 100 µL of 2.4 µM SF solution spread on 1 × 1.5 cm quartz surface to ensure that the highest absorbance value was less than 1.5 O.D. CD measurements were further recorded from 620 to 450 nm with step size and bandwidth of 1 nm, in order to observe the RHD band. SF:RHD films with 1:2 and 1:5 ratios were used for these measurements. Four and six scans were averaged for far-UV and visible CD regions. All CD measurements were performed at room temperature (22 °C). To avoid artifacts CD spectra of the films were collected by rotating of 45° (eigth positions) and averaged. No sign of linear dichroism was observed in the films. The absence of linear dichroism effects in the films indicates that the films are isotropic (molecules do not have favorite orientation on the plane of the surface).

Fluorescence Spectroscopy: Fluorescence measurements for SF, SF:RHD (from 1:0.5 to 1:19) and RHD films, were performed with a Nanolog spectrofluorimeter with DeltaTime time correlated single photon counting equipped with a single-photon detection module PPD-850, single photon detector module with DeltaTimeserieDD-300 and DD-6L DeltaDiode sources at 300 and 407 nm. Time resolved measurements for SF:RHD (1:0.005), SF:RHD (1:0.02), and SF:RHD (1:0.2) were performed using FluoTime 300 (PicoQuant, Germany) using front face accessory. Excitation source was picoseconds LED with wavelength max at about 340 nm. Intensity decays were measured at maximum of fluorescence using slitwidth of 10 nm. Instrument software was used for data analysis. The intensity decay data were analyzed in terms of the multiexponential decay law:

$$I(t) = \sum_i \alpha_i \exp\left(-\frac{t}{\tau_i}\right)$$

where α_i and τ_i are the normalized pre-exponential factors and decay times, respectively. The fractional fluorescence intensity of each component is defined as $f_i = \alpha_i \tau_i / \sum_j \alpha_j \tau_j$. Intensity (mean lifetime) and amplitude-averaged (corresponding to quantum yield) lifetimes were calculated as $\tau_{aver} = \sum_i f_i \tau_i$ and $\langle \tau \rangle = \sum_i \alpha_i \tau_i$ respectively. The quality of the fit was evaluated by the χ^2 criterion.

UV–Vis Absorption Analysis: UV–vis absorption spectra were measured using Shimadzu UV-2700 spectrophotometer. Spectral slitwidth was set 1.0 nm. Spectral manipulations and Gaussian multi component fitting was performed using OriginLab software. To report area-normalized absorption spectra, specific region of the absorption spectra (430–610 nm), with various RHD concentrations, were digitally integrated and, then, the amplitudes of the spectra were modified to have the same area under the absorption curve.

Supporting Information

Supporting Information is available from the Wiley Online Library or from the author.

Acknowledgements

L.R. and H.M. gratefully acknowledge Fondazione Antonio De Marco (Italy) and all authors acknowledge bilateral project CNR-Azerbaijan National Academy of Sciences (ANAS) for financial support. L.R. acknowledges Joint Project_2017 from the University of Verona (Prof. M. Assfalg) for financial support.

Conflict of Interest

The authors declare no conflict of interest.

Keywords

dye-doped biomaterials, exciton coupled CD, fluorescence, FTIR, silk fibroin

Received: October 19, 2018
Revised: December 19, 2018
Published online:

[1] Z. Shao, F. Vollrath, *Nature* **2002**, *418*, 741.
[2] C. Vepari, D. L. Kaplan, *Prog. Polym. Sci.* **2007**, *32*, 991.
[3] A. Matsumoto, J. Chen, A. L. Collette, U. J. Kim, G. H. Altman, P. Cebe, D. L. Kaplan, *J. Phys. Chem. B* **2006**, *110*, 21630.
[4] A. R. Murphy, D. L. Kaplan, *J. Mater. Chem.* **2009**, *19*, 6443.
[5] W. Huang, S. Ling, C. Li, F. G. Omenetto, D. L. Kaplan, *Chem. Soc. Rev.* **2018**, *47*, 6486.
[6] M. Farokhi, F. Mottaghitalab, Y. Fatahi, A. Khademhosseini, D. L. Kaplan, *Trends Biotechnol.* **2018**, *36*, 907.
[7] E. M. Pritchard, D. L. Kaplan, *Expert Opin. Drug Delivery* **2011**, *8*, 797.
[8] L. D. Koh, J. Yeo, Y. Y. Lee, Q. Ong, M. Han, B. C. Tee, *Mater. Sci. Eng., C* **2018**, *86*, 151.
[9] M. V. Santos, E. Pecoraro, S. H. Santagneli, A. L. Moura, M. Cavicchioli, V. Jerez, L. A. Rocha, L. F. C. de Oliveira, A. S.

L. Gomes, C. B. de Araujo, S. J. L. Ribeiro, *J. Mater. Chem. C* **2018**, *6*, 2712.
[10] R. R. da Silva, M. Cavicchioli, L. R. Lima, C. G. Otoni, H. S. Barud, S. H. Santagneli, A. Tercjak, A. C. Amaral, R. A. Carvalho, S. J. L. Ribeiro, *ACS Appl. Mater. Interfaces* **2017**, *9*, 18.
[11] Z. Zhou, Z. Shi, X. Cai, S. Zhang, S. G. Corder, X. Li, Y. Zhang, G. Zhang, L. Chen, M. Liu, D. L. Kaplan, F. G. Omenetto, Y. Mao, Z. Tao, T. H. Tao, *Adv. Mater.* **2017**, *29*.
[12] B. D. Lawrence, M. Cronin-Golomb, I. Georgakoudi, D. L. Kaplan, F. G. Omenetto, *Biomacromolecules* **2008**, *9*, 1214.
[13] F. G. Omenetto, D. L. Kaplan, *Science* **2010**, *329*, 528.
[14] F. G. Omenetto, D. L. Kaplan, *Nat. Photonics* **2008**, *2*, 641.
[15] S. Tomaselli, U. Giovanella, K. Pagano, G. Leone, S. Zanzoni, M. Assfalg, F. Meinardi, H. Molinari, C. Botta, L. Ragona, *Biomacromolecules* **2013**, *14*, 3549.
[16] L. Ragona, O. Gasymov, A. J. Guliyeva, R. B. Aslanov, S. Zanzoni, C. Botta, H. Molinari, *Biochim. Biophys. Acta, Proteins Proteomics* **2018**, *1866*, 661.
[17] U. Shimanovich, D. Pinotsi, K. Shimanovich, N. Yu, S. Bolisetty, J. Adamcik, R. Mezzenga, J. Charmet, F. Vollrath, E. Gazit, C. M. Dobson, G. K. Schierle, C. Holland, C. F. Kaminski, T. P. J. Knowles, *Macromol. Biosci.* **2018**, *18*, 1700295.
[18] R. R. Da Silva, C. T. Dominguez, M. V. dos Santos, R. Barbosa-Silva, M. Cavicchioli, L. M. Christovan, L. S. A. de Melo, A. S. L. Gomes, C. B. de Araujo, S. J. L. Ribeiro, *J. Mater. Chem. C* **2013**, *1*, 7181.
[19] H. J. Jin, J. Park, V. Karageorgiou, U. J. Kim, R. Valluzzi, D. L. Kaplan, *Adv. Funct. Mater.* **2005**, *15*, 1241.
[20] E. M. Pritchard, P. B. Dennis, F. Omenetto, R. R. Naik, D. L. Kaplan, *Biopolymers* **2012**, *97*, 479.
[21] A. Pistone, A. Sagnella, C. Chieco, G. Bertazza, G. Varchi, F. Formaggio, T. Posati, E. Saracino, M. Caprini, S. Bonetti, S. Toffanin, N. Di Virgilio, M. Muccini, F. Rossi, G. Ruani, R. Zamboni, V. Benfenati, *Biopolymers* **2016**, *105*, 287.
[22] S. W. Ha, A. E. Tonelli, S. M. Hudson, *Biomacromolecules* **2005**, *6*, 1722.
[23] D. J. Belton, R. Plowright, D. L. Kaplan, C. C. Perry, *Acta Biomater.* **2018**, *73*, 355.
[24] B. D. Lawrence, S. Wharram, J. A. Kluge, G. G. Leisk, F. G. Omenetto, M. I. Rosenblatt, D. L. Kaplan, *Macromol. Biosci.* **2010**, *10*, 393.
[25] M. Bouchard, J. Zurdo, E. J. Nettleton, C. M. Dobson, C. V. Robinson, *Protein Sci.* **2000**, *9*, 1960.
[26] T. Luhrs, C. Ritter, M. Adrian, D. Riek-Loher, B. Bohrmann, H. Dobeli, D. Schubert, R. Riek, *Proc. Natl. Acad. Sci.* USA **2005**, *102*, 17342.
[27] S. D. Moran, M. T. Zanni, *J. Phys. Chem. Lett.* **2014**, *5*, 1984.
[28] H.-J. Jin, J. Park, V. Karageorgiou, U.-J. Kim, R. Valluzzi, P. Cebe, D. L. Kaplan, *Adv. Funct. Mater.* **2005**, *15*, 1241.
[29] S. Dutta, B. Talukdar, R. Bharali, R. Rajkhowa, D. Devi, *Biopolymers* **2013**, *99*, 326.
[30] R. Valluzzi, H. J. Jin, *Biomacromolecules* **2004**, *5*, 696.
[31] V. M. Martınez, F. L. Arbeloa, J. B. Prieto, T. A. Lopez, I. L. Arbeloa, *J. Phys. Chem. B* **2004**, *108*, 8.
[32] M. F. Pouet, E. Baures, S. Vaillant, O. Thomas, *Appl. Spectrosc.* **2004**, *58*, 486.
[33] D. Toptygin, B. Z. Packard, L. Brand, *Chem. Phys. Lett.* **1997**, *277*, 430.
[34] N. Harada, K. Nakanishi, *Circular Spectroscopy: Exciton Coupling in Organic Stereochemistry*, University Science Books, Mill Valley, CA **1983**.
[35] I. B. Grishina, R. W. Woody, *Faraday Discuss.99*, **1994**, 245.
[36] R. W. Woody, *Eur. Biophys. J.* **1994**, *23*, 253.
[37] N. Harada, K. Nakanishi, N. Berova, *Electronic CD Exciton Chirality Method: Principles and Applications*, John Wiley & Sons, Hoboken, NJ **2012**.
[38] N. Sreerama, R. W. Woody, *Methods Enzymol.* **2004**, *383*, 318.
[39] O. K. Gasymov, A. R. Abduragimov, T. N. Yusifov, B. J. Glasgow, *Biochemistry* **2002**, *41*, 8837.
[40] M. A. Khan, C. Neale, C. Michaux, R. Pomes, G. G. Prive, R. W. Woody, R. E. Bishop, *Biochemistry* **2007**, *46*, 4565.
[41] O. K. Gasymov, A. R. Abduragimov, B. J. Glasgow, *J. Phys. Chem. B* **2015**, *119*, 3962.
[42] U. Shimanovich, D. Pinotsi, K. Shimanovich, N. Yu, S. Bolisetty, J. Adamcik, R. Mezzenga, J. Charmet, F. Vollrath, E. Gazit, C. M. Dobson, G. K. Schierle, C. Holland, C. F. Kaminski, T. P. J. Knowles, *Macromol. Biosci.* **2018**, *18*, e1700295.
[43] I. Georgakoudi, I. Tsai, C. Greiner, C. Wong, J. Defelice, D. Kaplan, *Opt. Express* **2007**, *15*, 1043.
[44] B. P. Partlow, M. Bagheri, J. L. Harden, D. L. Kaplan, *Biomacromolecules* **2016**, *17*, 3570.
[45] V. Martinez-Martinez, F. Lopez-Arbeloa, J. Banuelos Prieto, I. Lopez-Arbeloa, *J. Phys. Chem. B* **2005**, *109*, 7443.
[46] F. L. Arbeloa, P. R. Ojeda, I. L. Arbeloa, *J. Chem. Soc., Faraday Trans. 2* **1988**, *84*, 10.
[47] J. R. Lakowicz, *Principles of Fluorescence Spectroscopy*, 3rd ed., Kluwer Academic/Plenum Publishers, NY **2006**.
[48] A. C. Vaiana, H. Neuweiler, A. Schulz, J. Wolfrum, M. Sauer, J. C. Smith, *J. Am. Chem. Soc.* **2003**, *125*, 14564.
[49] J. M. Steves, L. T. Tan, J. A. Gardella, Jr., R. Hard, W. L. Hicks, Jr., A. N. Cartwright, B. Koc, F. V. Bright, *Appl. Spectrosc.* **2008**, *62*, 290.
[50] S. G. Lopez, G. Worringer, H. B. Rodriguez, E. San Roman, *Phys. Chem. Chem. Phys.* **2010**, *12*, 2246.
[51] S. T. Parker, P. Domachuk, J. Amsden, J. Bressner, J. A. Lewis, D. L. Kaplan, F. G. Omenetto, *Adv. Mater.* **2009**, *21*, 2411.
[52] S. Caixeiro, M. Gaio, B. Marelli, F. G. Omenetto, R. Sapienza, *Adv. Opt. Mater.* **2016**, *4*, 998.
[53] S. Kim, S. Yang, S. H. Choi, Y. L. Kim, W. Ryu, C. Joo, *Sci. Rep.* **2017**, *7*, 4506.
[54] V. Kalaparthi, S. Palantavida, I. Sokolov, *J. Mater. Chem. C* **2016**, *4*, 2197.
[55] R. Sola-Llano, Y. Fujita, L. Gomez-Hortiguela, A. Alfayate, I. H. Uji, E. Fron, S. Toyouchi, J. Perez-Pariente, I. Lopez-Arbeloa, V. Martinez-Martinez, *ACS Photonics* **2018**, *5*, 151.
[56] M. Busby, A. Devaux, C. Blum, V. Subramaniam, G. Calzaferri, L. De Cola, *J. Phys. Chem. C* **2011**, *115*, 5974.
[57] C. Botta, G. Patrinoiu, P. Picouet, S. Yunus, J. E. Communal, F. Cordella, F. Quochi, A. Mura, G. Bongiovanni, M. Pasini, S. Destri, G. Di Silvestro, *Adv. Mater.* **2004**, *16*, 1716.
[58] K. Yazawa, K. Ishida, H. Masunaga, T. Hikima, K. Numata, *Biomacromolecules* **2016**, *17*, 1057.

Supporting Information

for *Macromol. Chem. Phys.,* DOI: 10.1002/macp.201800460

Silk Fibroin-Based Films Enhance Rhodamine 6G Emission in the Solid State: A Chemical–Physical Analysis of their Interactions for the Design of Highly Emissive Biomaterials

Oktay K. Gasymov,* Chiara Botta, Laura Ragona, Aytaj J. Guliyeva, and Henriette Molinari*

Supporting Information

Silk fibroin-based films enhance Rhodamine 6G emission in the solid state: a chemical-physical analysis of their interactions for the design of highly emissive biomaterials

Oktay K. Gasymov[1]*, Chiara Botta[2], Laura Ragona[2], Aytaj J. Guliyeva[1], Henriette Molinari[2]*

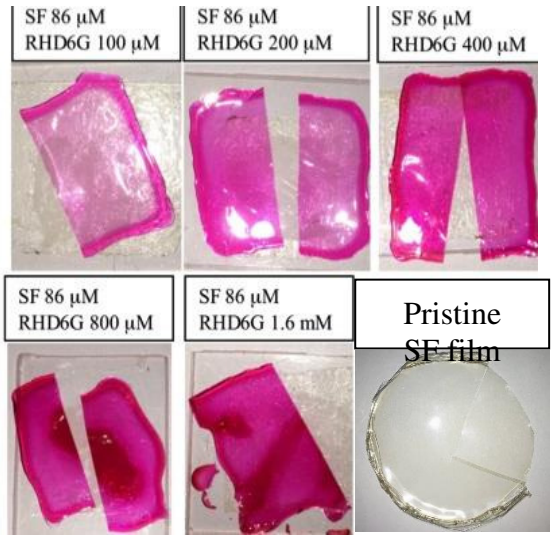

Figure S1. Images of the films obtained for SF:RHD films at different ratios. SF and RHD initial concentrations (in aqueous solution) used for film formation are indicated. For comparison, image of the pristine SF film is also shown.

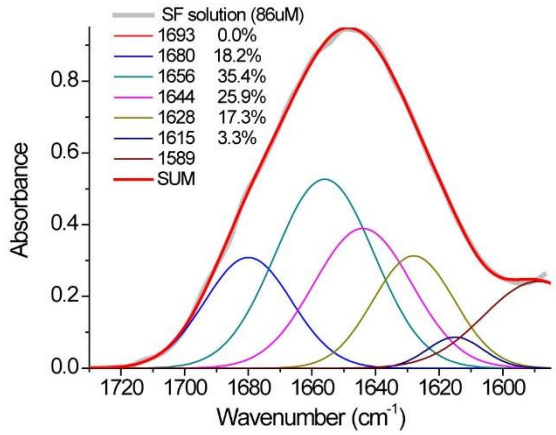
SF solution (86uM)
1693 0.0%
1680 18.2%
1656 35.4%
1644 25.9%
1628 17.3%
1615 3.3%
1589
SUM
Absorbance
Wavenumber (cm-1)

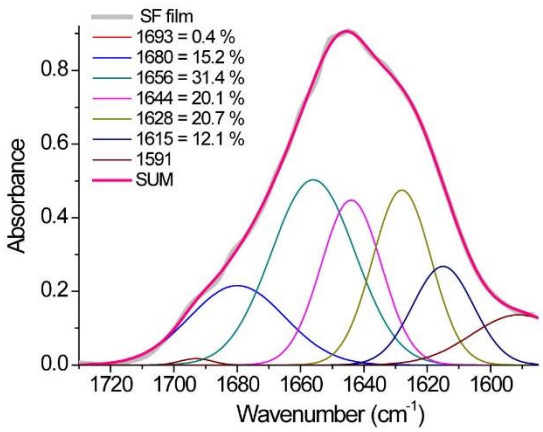
SF film
1693 = 0.4 %
1680 = 15.2 %
1656 = 31.4 %
1644 = 20.1 %
1628 = 20.7 %
1615 = 12.1 %
1591
SUM
Absorbance
Wavenumber (cm-1)

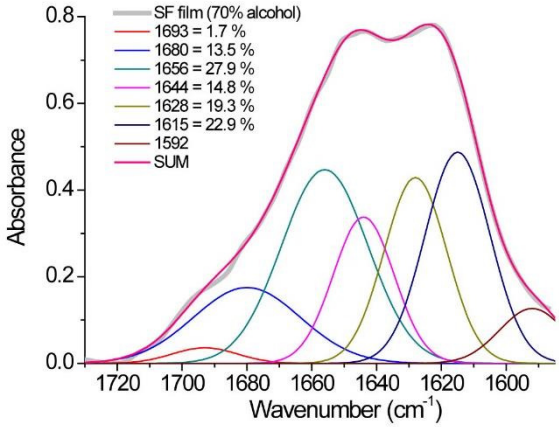
SF film (70% alcohol)
1693 = 1.7 %
1680 = 13.5 %
1656 = 27.9 %
1644 = 14.8 %
1628 = 19.3 %
1615 = 22.9 %
1592
SUM
Absorbance
Wavenumber (cm-1)

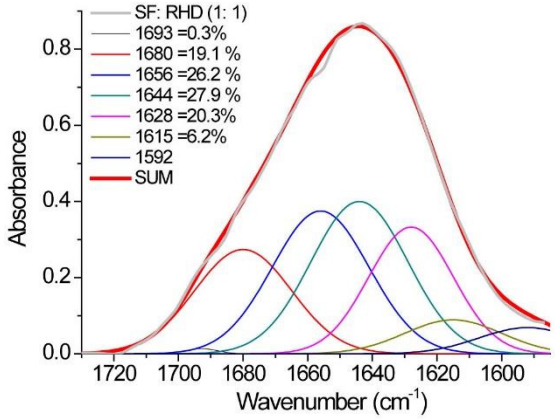
SF: RHD (1: 1)
1693 =0.3%
1680 =19.1 %
1656 =26.2 %
1644 =27.9 %
1628 =20.3%
1615 =6.2%
1592
SUM
Absorbance
Wavenumber (cm-1)

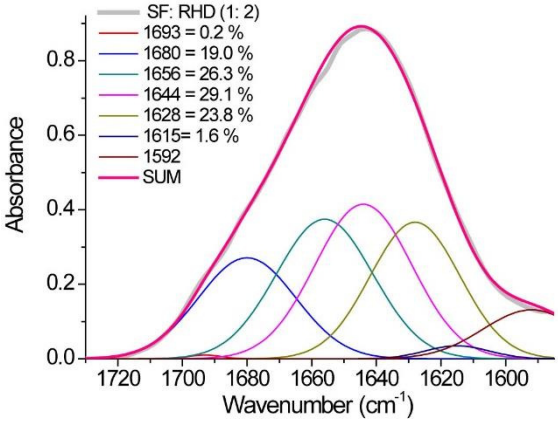
SF: RHD (1: 2)
1693 = 0.2 %
1680 = 19.0 %
1656 = 26.3 %
1644 = 29.1 %
1628 = 23.8 %
1615= 1.6 %
1592
SUM
Absorbance
Wavenumber (cm-1)

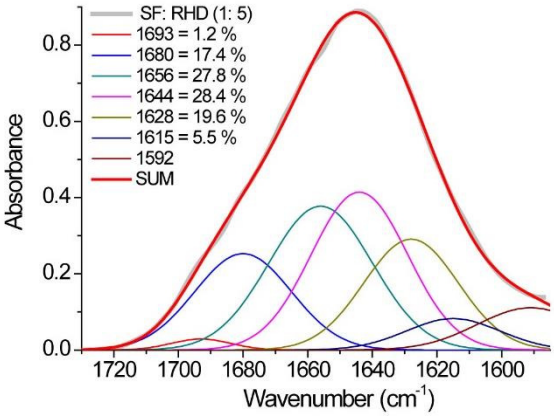
SF: RHD (1: 5)
1693 = 1.2 %
1680 = 17.4 %
1656 = 27.8 %
1644 = 28.4 %
1628 = 19.6 %
1615 = 5.5 %
1592
SUM
Absorbance
Wavenumber (cm-1)

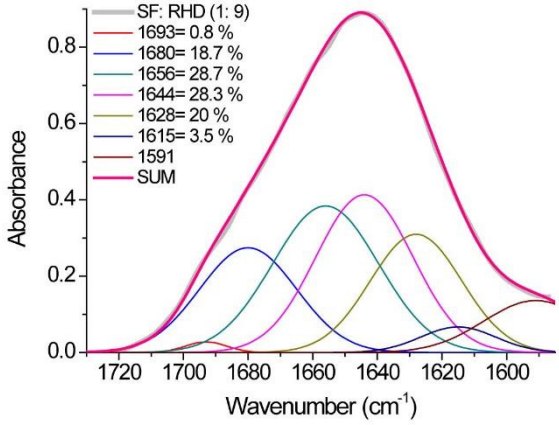
SF: RHD (1: 9)
1693= 0.8 %
1680= 18.7 %
1656= 28.7 %
1644= 28.3 %
1628= 20 %
1615= 3.5 %
1591
SUM
Absorbance
Wavenumber (cm-1)

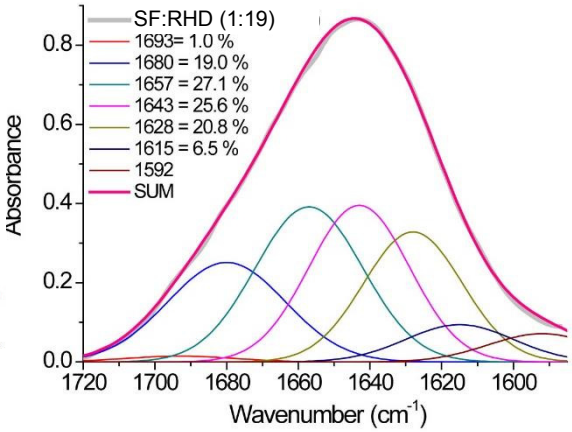
SF:RHD (1:19)
1693= 1.0 %
1680 = 19.0 %
1657 = 27.1 %
1643 = 25.6 %
1628 = 20.8 %
1615 = 6.5 %
1592
SUM
Absorbance
Wavenumber (cm-1)

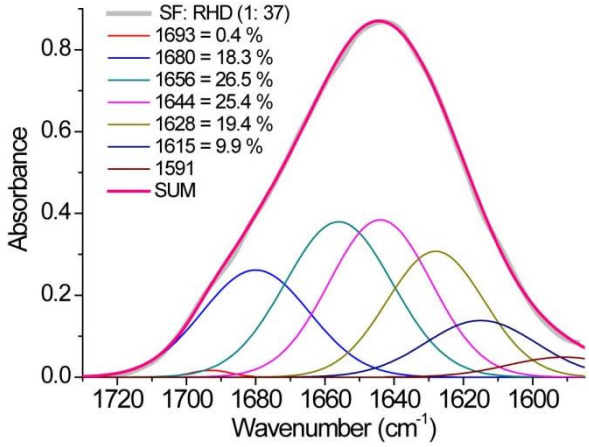
SF: RHD (1: 37)
1693 = 0.4 %
1680 = 18.3 %
1656 = 26.5 %
1644 = 25.4 %
1628 = 19.4 %
1615 = 9.9 %
1591
SUM
Absorbance
Wavenumber (cm-1)

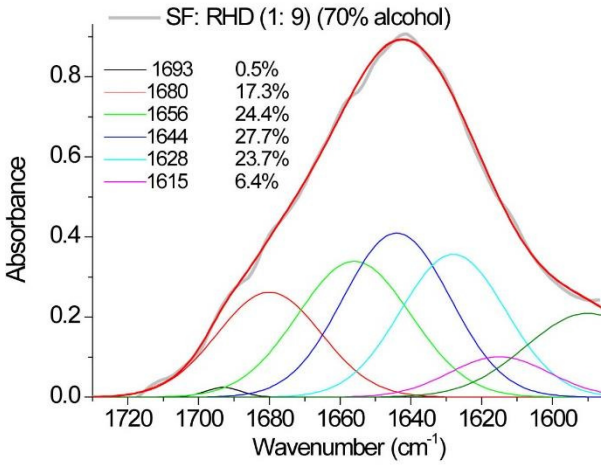
SF: RHD (1: 9) (70% alcohol)
1693 0.5%
1680 17.3%
1656 24.4%
1644 27.7%
1628 23.7%
1615 6.4%
Absorbance
Wavenumber (cm-1)

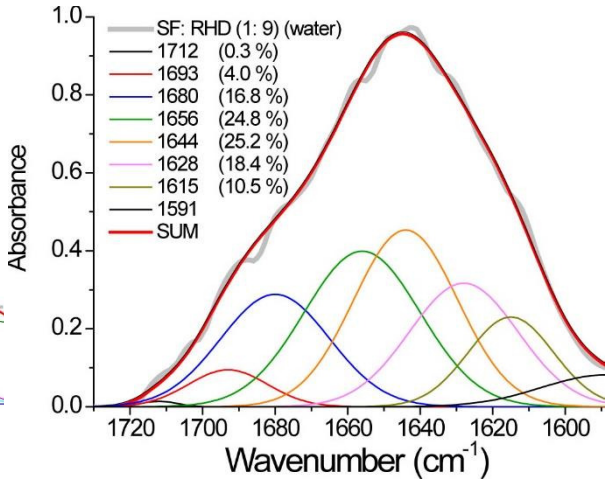
SF: RHD (1: 9) (water)
1712 (0.3 %)
1693 (4.0 %)
1680 (16.8 %)
1656 (24.8 %)
1644 (25.2 %)
1628 (18.4 %)
1615 (10.5 %)
1591
SUM
Absorbance
Wavenumber (cm-1)

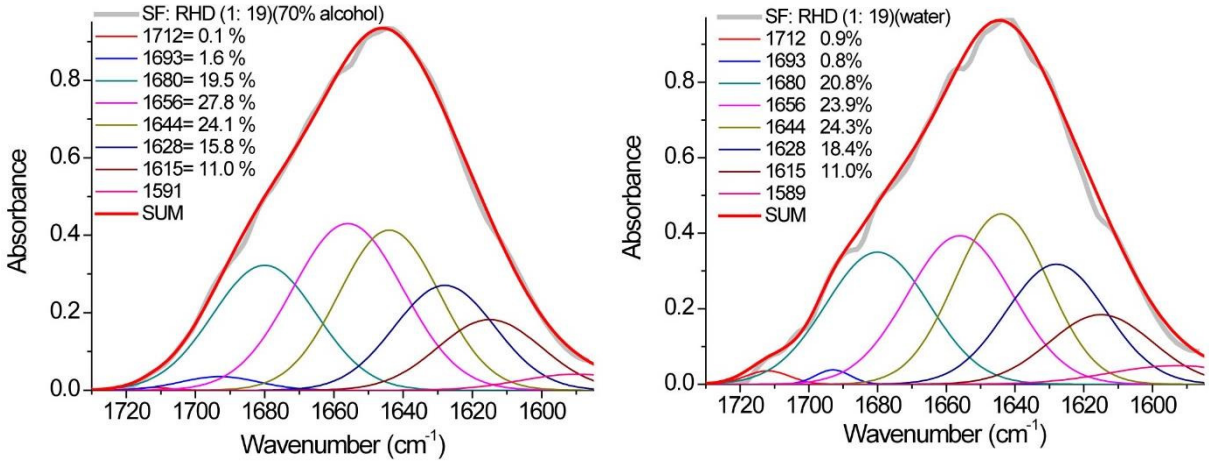

Figure S2. Deconvolution of the amide I bands of the films reported in Figure 2.

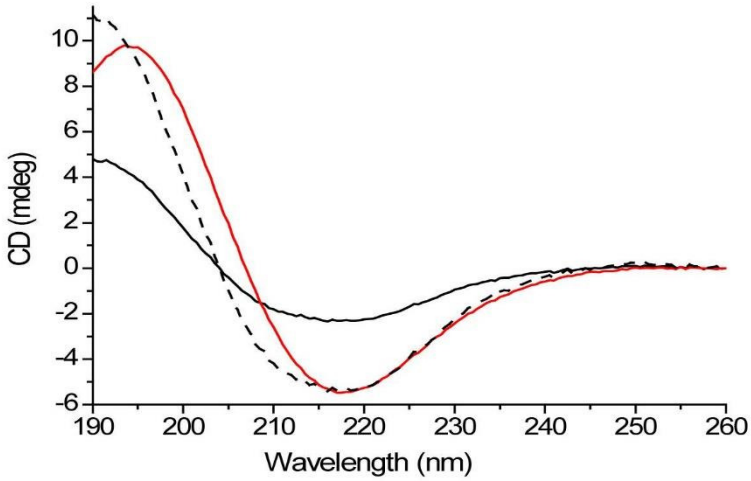

Figure S3. CD spectra of SF films. SF film prepared from 100 μL of 2.4 μM SF solution spread on 1x1.5 cm quartz surface (black line); SF film treated with alcohol (red line); the amplitude of SF film has been normalized to that of SF film treated with alcohol (black dashed line) to highlight changes in spectral shape. CD spectrum of the pristine SF film exhibits a broad negative band at 216 nm and a positive band at 190.5 nm, while, after alcohol treatment, a narrower and more intense negative band is observed at 217.6 nm with a positive band at 194.1 nm. Almost identical CD spectra were obtained for insulin amyloid fibrils (M. Bouchard, J. Zurdo, E. J. Nettleton, C. M. Dobson, C. V. Robinson, Protein Sci **2000**, 9, 1960) thus confirming that silk fibroin can be considered a good model of β-amyloid fibril formation.

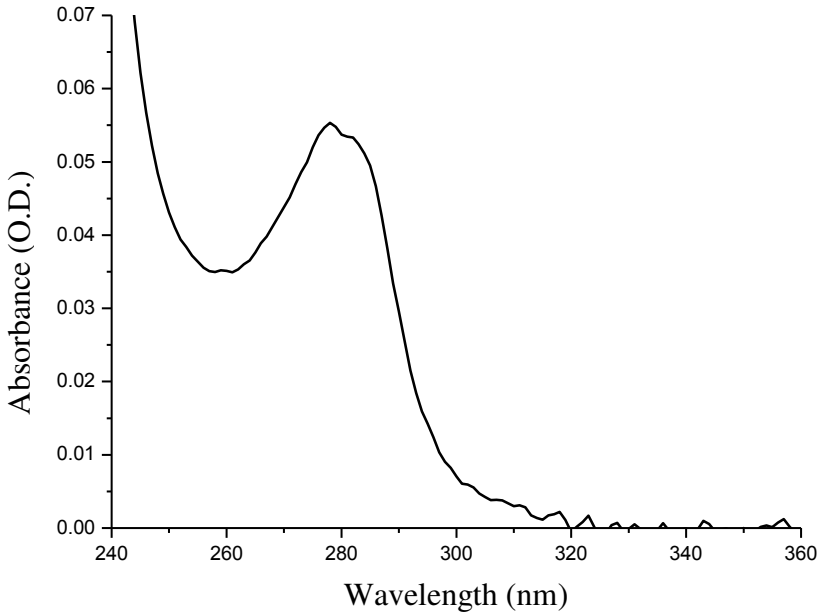

Figure S4. Absorption spectrum of a pristine SF film

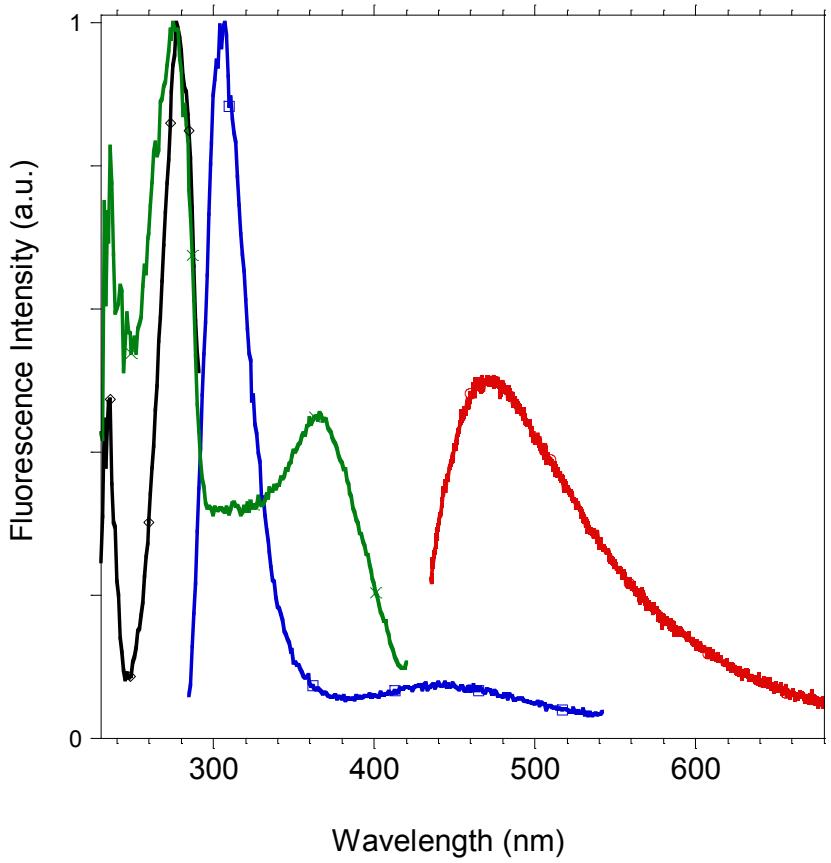

Figure S5. Fluorescence emission (λ_{exc} = 275nm, blue line; λ_{exc} = 407 nm, red line) and fluorescence excitation (λ_{em} = 305nm, black line; λ_{em} = 450nm, green line) spectra of SF film.

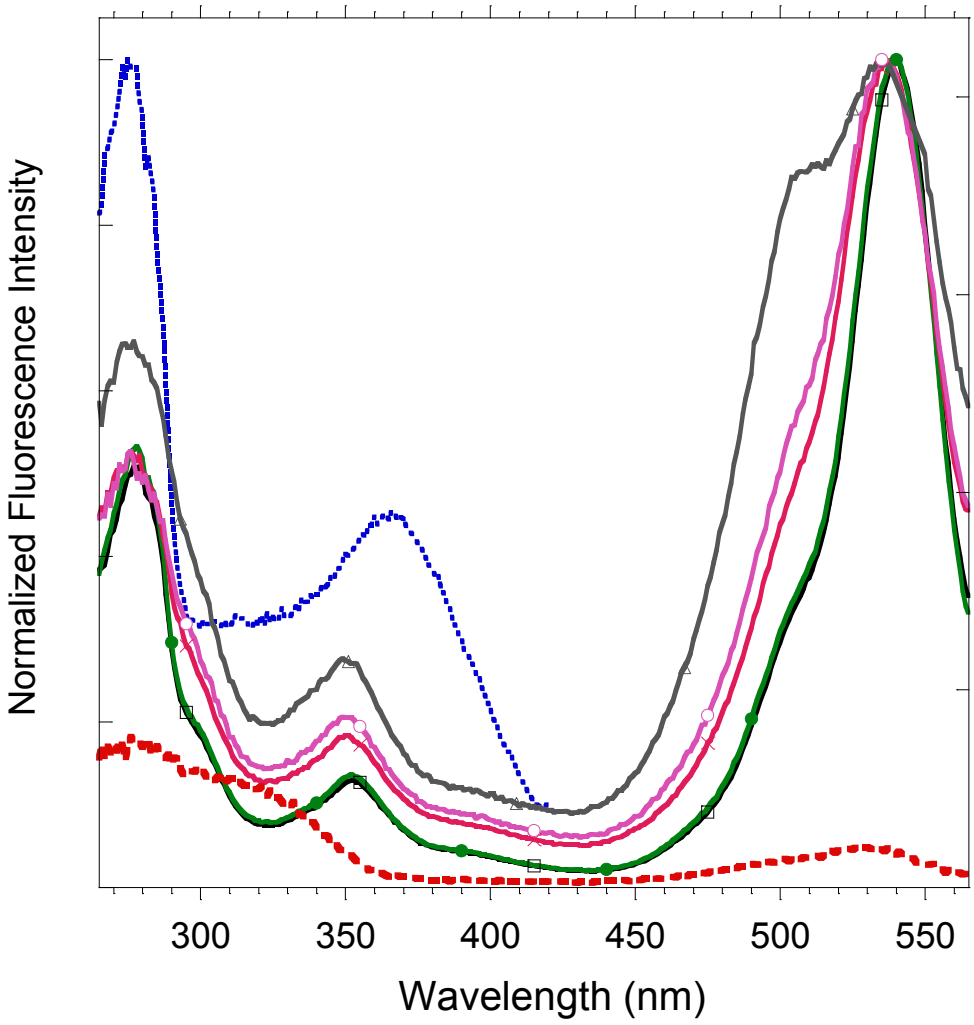

Figure S6. Fluorescence excitation spectra of SF:RHD films at different molar ratios (1:0, blue dotted line; 1:0.5 black line; 1:1 green line; 1:5 red line; 1:10 pink line; 1:20 grey line; 0:1 red dashed line).

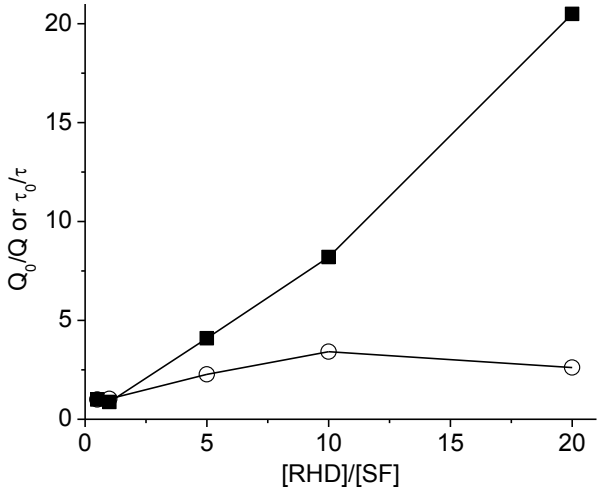

Figure S7. Concentration dependence of the fluorescence quantum yield and lifetime of RHD in the various SF:RHD films. Solid squares and open circles represent Q_0/Q and τ_0/τ, respectively.

Figure S8: Demountable sandwich cell for fluorescence measurements of hydrated SF:RHD films. Teflon plate of 0.3 mm thickness with a square hole is sandwiched between two quartz plates to prevent evaporation of the hydrated samples. The thin hydrated film was positioned in the gap created by teflon plate. The cell holder is shown in a front (left picture) and side view (right picture).